Third Order Dispersion in Time-Delayed Systems

C. Schelte,[1,2] P. Camelin,[3] M. Marconi,[3] A. Garnache,[4] G. Huyet,[3] G. Beaudoin,[5] I. Sagnes,[5] M. Giudici,[3] J. Javaloyes,[1] and S. V. Gurevich[2,*]

[1]*Departament de Física & Institute of Applied Computing and Community Code (IAC-3),Universitat de les Illes Baleares, C/Valldemossa km 7.5, 07122 Mallorca, Spain*

[2]*Institute for Theoretical Physics, University of Münster, Wilhelm-Klemm-Str. 9 & Center for Nonlinear Science (CeNoS), University of Münster, Corrensstrasse 2, D-48149 Münster, Germany*

[3]*Université Côte d'Azur, Centre National de La Recherche Scientifique, Institut de Physique de Nice, F-06560 Valbonne, France*

[4]*Institut d'Électronique et des Systèmes (IES), Centre National de La Recherche Scientifique UMR 5214, Univ. Montpellier, 34095 Montpellier, France*

[5]*Centre de Nanosciences et de Nanotechnologies, Centre National de La Recherche Scientifique UMR 9001, Université Paris-Saclay, 91120 Palaiseau, France*

(Received 6 February 2019; revised manuscript received 10 May 2019; published 26 July 2019)

Time-delayed dynamical systems materialize in situations where distant, pointwise, nonlinear nodes exchange information that propagates at a finite speed. However, they are considered devoid of dispersive effects, which are known to play a leading role in pattern formation and wave dynamics. We show how dispersion may appear naturally in delayed systems and we exemplify our result by studying theoretically and experimentally the influence of third order dispersion in a system composed of coupled optical microcavities. Dispersion-induced pulse satellites emerge asymmetrically and destabilize the mode-locking regime.

DOI: 10.1103/PhysRevLett.123.043902

Delayed dynamical systems describe a large number of phenomena in nature and they exhibit a wealth of dynamical regimes such as localized structures, fronts and chimera states [1–8]. A fertile perspective lies in their interpretation as spatially extended *diffusive* systems which holds in the limit of long delays [9]. The presence of delayed terms is connected with the finite propagation speed of signals; hence delayed systems are widely used to model, e.g., networks, map lattices or optical systems; see Ref. [10] for a review. A strong limitation of delayed dynamical systems for modeling optical systems comes from the difficulty of taking into consideration chromatic dispersion which describes the dephasing of the spectral components of a wave packet, thus making the delayed terms frequency dependent. As such, description of wave propagation via delayed models is limited to weakly dispersive media and/or signals with narrow spectral bandwidth. Nevertheless, chromatic dispersion plays a leading role in many phenomena occurring during wave evolution. In particular, second order dispersion in nonlinear extended media governs the Benjamin-Feir (modulational) instability [11] and also controls the appearance of cavity solitons in injected Kerr fibers [12]. Third order dispersion is the lowest order nontrivial parity symmetry breaking effect, which leads to convective instabilities [13–15] and drifts [16–18]. Wave propagation in dispersive media can be described by partial differential equations both in conservative and dissipative frameworks using, for instance, the nonlinear Schrödinger or the complex Ginzburg-Landau equations. However, the possibility of describing dispersive phenomena using delayed dynamical systems is very attractive because it would allow reducing the complexity of models based upon partial differential equations, while still allowing for extended bifurcation analysis. For example, the time-delayed description of laser mode locking developed in Ref. [19] allowed for the bifurcation analysis of pulsed solutions but also to unveil their connections with all the other possible solutions. This analysis is out of the reach of pulse iterative models based upon partial differential equations as in Ref. [20]. Recently, a complex procedure involving integro-differential equations has been developed for taking into account dispersion in time-delayed systems [11,21]. However the description of dispersion as a simple, robust, and unitary transformation in delayed systems framework remained elusive so far.

In this Letter we show that second and third order dispersion appear naturally when modeling a singularly perturbed time-delayed system. The latter materialize in the modeling of Vertical External-Cavity Surface-Emitting Lasers (VECSELs) and we illustrate our general result studying the effect of third order dispersion on the optical pulses found in the output of a passively mode-locked VECSEL. We show that third order dispersion leads to the creation of satellites on one edge of the pulse which induces a new form of pulse instability. Our results are in good agreement with some experimental observations.

Consider a linear time-delayed system for a scalar field $y(t)$,

$$M\frac{dy}{dt} = Ay(t) + By(t-\tau), \tag{1}$$

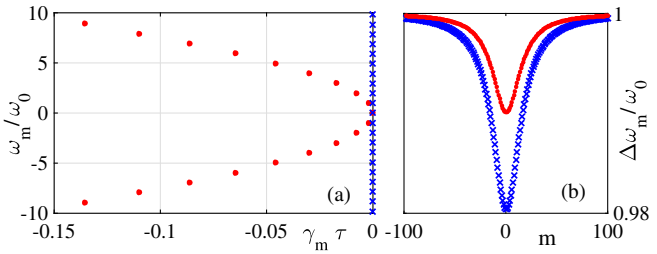

FIG. 1. (a) Eigenvalue spectrum of Eq. (1) for $A=-1$, $B=M=1$ (red circles) and for $\mathbf{A}=(-1,2;0,-1)$, $\mathbf{B}=(0,0;1,-1)$ and $\mathbf{M}=\mathrm{diag}(1,0)$ (blue crosses). We represent the real part of the eigenvalues γ_m (normalized to the time delay τ) as well as the imaginary part ω_m normalized to the nominal separation ω_0. In the absence of chromatic dispersion, ω_m/ω_0 would be an integer. (b) Normalized separation of the imaginary part of the eigenvalue $\Delta\omega_m/\omega_0$ as a function of the index m. Departure from unity indicates chromatic dispersion. For both cases, $\tau=100$.

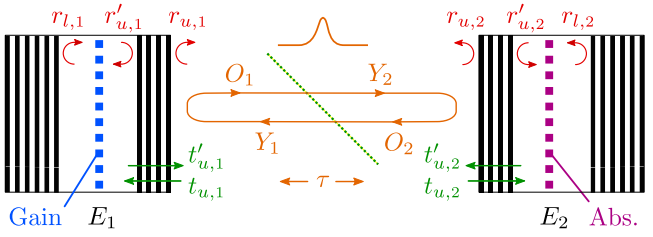

FIG. 2. A schematic of the coupled cavities configuration. E_j denote the intracavity fields, $j=1,2$. The output and input fields in the external cavity are represented by O_j and Y_j, respectively. The time of flight in the cavity is τ.

with M, A, and B some real coefficients. Because of the presence of a time delay, Eq. (1) corresponds to a dynamical system with infinitely many degrees of freedom and its eigenvalue spectrum $\{\lambda_m=\gamma_m+i\omega_m\}$ is a countably infinite set. In the long delay limit $\tau\gg 1$, the spectrum becomes quasicontinuous [22] and the separation between the imaginary part of consecutive eigenvalues is a small, almost constant quantity, which we define as $\omega_0=2\pi/\tau\ll 1$, i.e., $\Delta\omega_m=\omega_{m+1}-\omega_m\simeq\omega_0$. For small values of m, the dissipative part γ_m of the spectrum shown in Fig. 1(a) (red circles) features a clear parabolic shape, thus evidencing the similarity between DDSs and spatially extended diffusive systems [9].

This generic situation can be modified drastically by extending Eq. (1) to a vectorial field $\mathbf{y}$ *and* for a particular choice of the 2×2 matrices $\mathbf{M}$, $\mathbf{A}$, and $\mathbf{B}$. Without loss of generality we set $\mathbf{M}=M_\varepsilon=\mathrm{diag}(1,\varepsilon)$ as well as $\mathbf{A}=(-1,h;0,-1)$ and $\mathbf{B}=(0,0;\eta,-\eta)$. The singular case $\varepsilon=0$ is of particular interest as one of the two delay differential equations becomes a delay algebraic equation. If, in addition, one sets $h=2$ and $\eta=1$, one obtains a *purely imaginary* eigenvalue spectrum $\{\lambda_m=i\omega_m\}$ typical of reversible systems, as shown in Fig. 1(a) (blue crosses) (see the Supplemental Material [23] for the analytical form of the eigenvalues). In this situation, where dissipation is canceled, the deviations of $\Delta\omega_m$ with respect to a perfectly regular comb with separation ω_0—i.e., chromatic dispersion—can influence the dynamics; the various waves in an initial wave packet have time to get dephased since they are not absorbed.

The normalized frequency separation $\Delta\omega_m/\omega_0$ for the two aforementioned cases is represented in Fig. 1(b). One notices for $m<0$ ($m>0$) a monotonic decrease (increase) of $\Delta\omega_m$. This corresponds to normal and anomalous second order dispersion, respectively, while, around $m=0$, the second order contribution vanishes, thus leaving third order dispersion as the dominant effect [24]. In conclusion, the two curves in Fig. 1(b) indicate that time-delayed systems are in fact generically both diffusive *and* dispersive, but that diffusion usually overwhelms dispersive effects.

These general considerations materialize when modeling a VECSEL as depicted in Fig. 2. Our theoretical approach follows the method developed in Refs. [25–28]. The dynamical model for the intracavity fields E_j and population inversions N_j reads

$$\kappa_1^{-1}\dot{E}_1=[(1-i\alpha_1)N_1-1]E_1+h_1Y_1, \tag{2}$$

$$\kappa_2^{-1}\dot{E}_2=[(1-i\alpha_2)N_2-1+i\delta]E_2+h_2Y_2, \tag{3}$$

$$\dot{N}_1=\gamma_1(J_1-N_1)-|E_1|^2N_1, \tag{4}$$

$$\dot{N}_2=\gamma_2(J_2-N_2)-s|E_2|^2N_2. \tag{5}$$

The indexes $j=1$, 2 denote a gain mirror and a semiconductor saturable absorber mirror (SESAM), respectively. The photon lifetimes are κ_j^{-1}, the detuning between the two cavities is δ, α_j denote the linewidth enhancement factors, and γ_j^{-1} are the population lifetimes. The forward and reverse bias of the gain and the saturable absorber are noted J_1 and J_2, respectively. The lasing threshold is defined as J_{th} and emission occurs for $J_1\geq J_{\mathrm{th}}$. The ratio of the gain and absorber saturation intensities is s. The fields injected into the microcavities are Y_j with a coupling factor given by $h_j=(1+|r_{l,j}|)(1-|r_{u,j}|)/(1-|r_{u,j}r_{l,j}|)$ with $r_{u,j}$ and $r_{l,j}$ the upper and lower distributed Bragg mirror reflectivities (in amplitude). The cavity outputs consist in a superposition between the reflected and emitted fields and read, after proper normalization, $O_j=E_j-Y_j$. As such, considering the time of flight between the two microcavities τ as well as the presence of the beam sampler with transmission amplitude t_{bs}, we find that the mutual injection between the two cavities is given by two delay algebraic equations

$$Y_1(t)=O_2(t-\tau)=t_{\mathrm{bs}}[E_2(t-\tau)-Y_2(t-\tau)], \tag{6}$$

$$Y_2(t)=O_1(t-\tau)=t_{\mathrm{bs}}[E_1(t-\tau)-Y_1(t-\tau)]. \tag{7}$$

For a perfectly reflecting upper mirror with zero transmission, we have $|r_{u,j}|=1$ and $h_j=0$, while a

symmetrical cavity for which $|r_{l,j}| = |r_{u,j}|$ yields $h_j = 1$. Interestingly, if $r_{l,j} \to 1$, we have $h_j \to 2$ and the cavity operates in the Gires-Tournois interferometer regime [29].

The (linear) characteristics of a single microcavity can be found setting $N_1 = 0$ in Eqs. (2), (7), and by replacing the other cavity by a partially reflecting mirror with reflectivity η. Here, one finds that the microcavity equations becomes formally identical to the time-delayed system for the vector field discussed in Eq. (1) setting $\mathbf{y} = (E_1, Y_1)^T$. In particular, the situation with $h_j = 2$ is of particular relevance since the bottom mirror of the microcavities is usually highly reflective and contains more stacked half-wavelength layers in order to minimize losses and increase emission directionality. Similar considerations apply also to the mode-locked integrated external-cavity surface emitting laser (MIXSEL) where both gain and absorber are located within the same microcavity.

The cavity response in reflection, as given by the relation $O_j = E_j - Y_j$, consists in the photons that are immediately reflected from the top mirror with a π phase shift, i.e., the $-Y_j$ term, and those that enter the cavity and remain trapped for an average duration that corresponds to the photon lifetime. Notice that the boundary conditions are dictating the delay algebraic equation structure of Eqs. (6), (7). The limit $\varepsilon \to 0$ of the matrix $\mathbf{M}_\varepsilon$, while helpful to understand the transition from diffusive (differential) toward dispersive (algebraic) delay equations in Eq. (2), is not an idealization and corresponds to a physical situation.

We apply the functional mapping method developed in Ref. [27] to link the field profiles in the external cavity $(E_1^{(n)}, Y_1^{(n)})$ at the nth round-trip to those of the previous one. We find

$$\tilde{E}_1^{(n)} = \frac{h_1 \tilde{Y}_1^{(n)}}{1 - i\omega}, \qquad \tilde{Y}_1^{(n)} = \eta(\tilde{E}_1^{(n-1)} - \tilde{Y}_1^{(n-1)}) \tag{8}$$

with $\tilde{X}(\omega)$ the Fourier transform of $X(t)$, $\eta = -t_{\mathrm{bs}}^2$ and $\kappa_1 = 1$ by a proper time normalization. Upon using that $h_1 = 2$, we find the following reflection coefficient

$$\tilde{Y}_1^{(n)} = \eta r_i(\omega) \tilde{Y}_1^{(n-1)}, \qquad r_i(\omega) = \exp\left[2i\theta(\omega)\right], \tag{9}$$

where we defined the complex reflectivity of the interferometer as $r_i(\omega)$ and $\theta(\omega) = \arctan \omega$. Besides the beam splitter attenuation factor η, one notices that the cavity response is unitary in Fourier space, since $|r_i| = 1$, meaning that all the photons are conserved irrespective of their wavelength. They are either directly reflected, or transmitted, stored, and reflected again. The filter is essentially dispersive and induces a phase shift that depends nonlinearly on the frequency.

The response of this linear system based upon delay algebraic equations is illustrated in Fig. 3 for the case of an incoming Gaussian pulse with varying full width at half maximum (FWHM). One notices, after each round-trip, the appearance of a new satellite over the leading edge of the pulse. As shown in Fig. 3, third order dispersion is a parity breaking effect that affects the pulse leading and falling edges differently. The interpretation of the emergence of satellites is direct, considering the expression of the cavity output O. One part of the response is immediate, while the other is delayed by the cavity band-pass filtering effect. The satellites are more visible for pulses whose width is close to (or smaller than) the cavity photon lifetime.

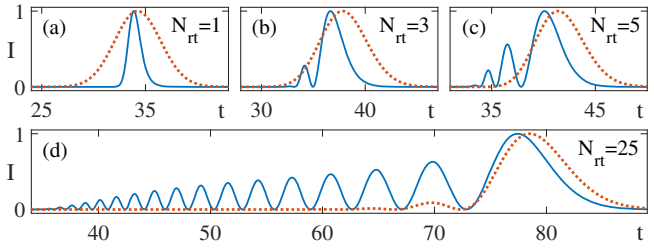

FIG. 3. Cavity response for two Gaussian pulses of FWHM $\tau_p = 1$ (blue line) and $\tau_p = 5$ (red dotted line) after a variable number of round-trips N_{rt}. At each round-trip, the total response consists of the superposition between the reflected and the filtered pulse inducing a train of satellites. The maximal intensity is normalized to unity for clarity.

Transforming back Eq. (9) into the time domain allows obtaining the field profile evolution from one round-trip towards the next. We define ξ as a slow timescale for the pulse evolution after each round-trip, such that $\partial_\xi \tilde{Y} = \ln\left[\eta r_i(\omega)\right]\tilde{Y}$. Upon expanding $\ln r_i(\omega)$ up to third order as $\ln r_i(\omega) = 2i \arctan(\omega) = 2i\omega - 2i/3\omega^3$ and reverting back to the time domain using that $-i\omega \to \partial_t$, we find that $Y(\xi, t)$ evolves according to

$$\frac{\partial Y}{\partial \xi} = \left(\ln \eta - 2\frac{\partial}{\partial t} - \frac{2}{3}\frac{\partial^3}{\partial t^3}\right) Y, \tag{10}$$

which allows us to identify the value of the third order dispersion and to emphasize the absence of second order diffusive and dispersive contributions. Gires-Tournois interferometers are usually used to induce a controllable amount of second order dispersion by operating them away from the cavity resonance, i.e., $\omega = 0$. Expanding $r_i(\omega)$ around a carrier frequency ω_0 and reverting to time domain for the slow amplitude setting $-i(\omega - \omega_0) \to \partial_t$ yields a second order dispersion contribution $+iD\partial_t^2 Y$ in Eq. (10) with coefficient $D = 2\omega_0/(1 + \omega_0^2)^2$.

In the presence of nonlinearity, writing a simple partial differential equation such as Eq. (10) may or may not be possible since nonlinearity and filtering are *a priori* nonseparable effects. However, because lasing occurs close to the cavity resonance $\omega = 0$, the lasing regime is essentially influenced by third order dispersion. Notwithstanding its limited applicability, Eq. (10) remains a useful qualitative tool to understand the dispersive response of Eqs. (2)–(7).

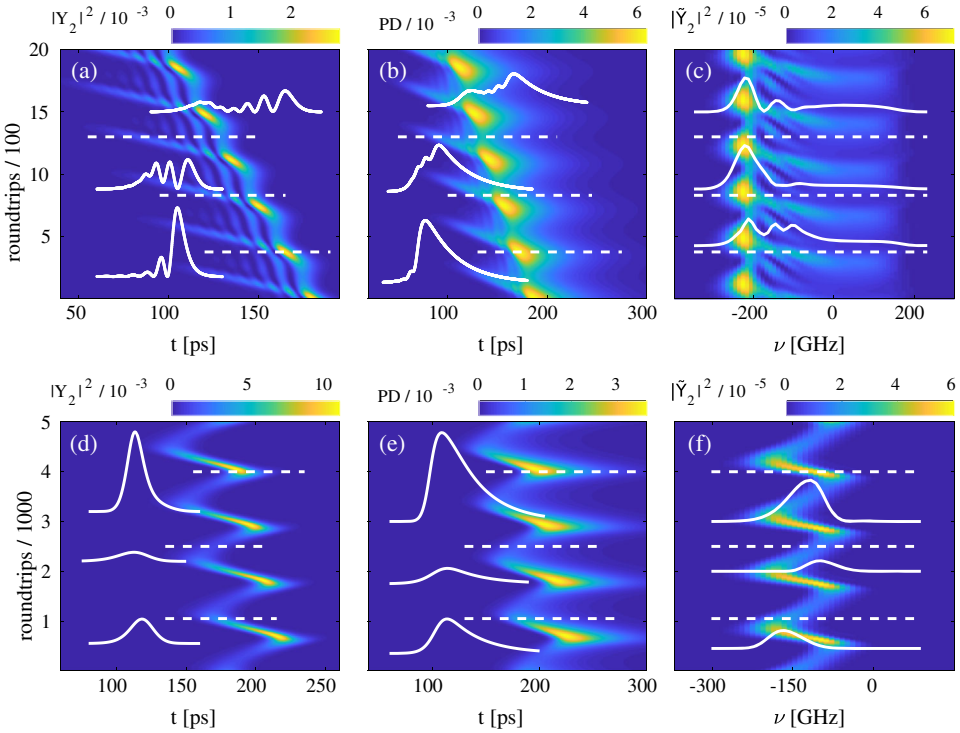

FIG. 4. Satellite instability regime found by direct numerical simulations of Eqs. (2), (7) for a single pulse. (a) Space-time diagram of the intensity. (b) Low-pass filtered @10 GHz detection. (c) Single round-trip optical spectrum. For sufficiently large gain the largest satellite is amplified, eventually replacing its parent pulse. Bias and parameters are $J_1 = 1.087 J_{\mathrm{th}}$, $(\kappa_1^{-1}, \kappa_2^{-1}, \gamma_1^{-1}, \gamma_2^{-1}, \tau) = (343\ \mathrm{fs}, 34.3\ \mathrm{fs}, 2.45\ \mathrm{ns}, 34\ \mathrm{ps}, 4.12\ \mathrm{ns})$, $(J_1, J_2, \alpha_1, \alpha_2, h_1, h_2) = (0.044, -0.03, 2.5, 1, 2, 1.9985)$, as well as $(t_{\mathrm{bs}}, s, \delta) = (0.985, 5.4, -0.5)$. (d),(e),(f) Deformed satellite instability for slightly different parameters $(J_1, \alpha_1, s) = (0.041, 2.3, 5.3)$. Here, $J_1 = 1.014 J_{\mathrm{th}}$. In both cases $J_{\mathrm{th}} \simeq 0.0404$.

Further, the coefficients of Eq. (10) can be directly mapped to the eigenvalues of the underlying Eq. (1), making the connection between partial differential equations with third order dispersion and delay algebraic equations feasible (see Supplemental Material [23]).

In the passive mode-locking regimes where short optical pulses are generated by the interplay between the nonlinear dynamics of gain and saturable absorption in the two cavities, the satellites on the leading edge do not experience net gain as their intensities are usually insufficient to bleach the saturable absorber. Hence, third order dispersion only perturbs the central pulse structure. Yet, in some situations, in particular for high bias current when the background zero intensity solution becomes weakly stable, one of the satellites, generally the one of highest intensity closest to the main pulse, can become linearly unstable and grow into a fully developed pulse. In this case, the newborn pulse will deprive the original pulse of gain, due to the finite recovery time of the carriers. This behavior can be interpreted as an *asymmetrical* soliton explosion [30–34]. Such a situation leads to the dynamics depicted in Fig. 4. The individual pulse dynamics are most readily observed using a so-called space-time diagram as in Fig. 4(a), where one can see the details of the pulse evolution over many round-trips. Here the growth of the satellites in front of the pulse, and the subsequent death of the original pulse is most visible and leads to an apparent motion of the pulse to the left. This ultrafast dynamics can be partially blurred by a photodetector having a limited bandwidth, but it remains visible; see Fig. 4(b). The optical spectrum is depicted in Fig. 4(c) where one can observe the evolving asymmetrical tail of the bluest side. A slightly different parameter set leads to deformed satellite explosions that resemble to an oscillation of the pulse position, see in Fig. 4(d). This oscillation remains visible even blurred by a photodetector as shown in Fig. 4(e). Oscillation of the optical spectrum can also be observed, cf., Fig. 4(f). In all cases, one notes the very long timescale of this dynamics that corresponds to the slow evolution of the satellite from one round-trip towards the next under the influence of nonlinearity, drift, and third order dispersion.

We have tested these theoretical predictions in a mode-locked VECSEL composed by a gain mirror and a SESAM placed at a distance of 15 cm leading to a cavity round-trip of $2\tau \approx 1$ ns. The experimental setup is described in the Supplemental Material [23] and it is similar to that of Ref. [28], while [35,36] used different imaging conditions. The gain mirror and SESAM are based on a GaAs substrate with a high reflectivity ($R \simeq 99.9\%$) bottom Bragg reflector: the first features 6 InGaAs/GaAsP quantum wells

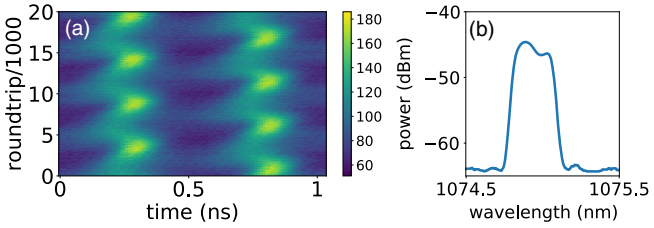

FIG. 5. (a) Experimental evidence of the satellite instability for two pulses in the same round-trip. Spatiotemporal diagram for the pulses evolution as a function of the number of cavity round-trips is shown. $J = 1.18J_{\mathrm{th}}$. (b) Time-averaged optical spectrum.

emitting at 1.06 μm [37,38], the second has a single InGaAs/GaAs quantum well [39]. The residual microcavity effects of the two devices have been controlled by adding few Bragg's pair on the top of the substrates. Accordingly, their finesse can be engineered for optimizing the level of maximum gain G and of saturable losses A at, respectively, the gain mirror and SESAM microcavities resonances (λ_G, λ_B). In the experiment described here, the microcavities bandwidths (FWHM) are $\Delta\lambda_G = 3.5$ nm for the gain mirror and $\Delta\lambda_B = 40$ nm for the SESAM and $A \approx 12\%$ at λ_B. Because $\Delta\lambda_G \ll \Delta\lambda_B$, the wavelength of the intracavity field is close to λ_G and the amount of saturable losses A depends ultimately on the detuning $\delta\lambda = \lambda_B - \lambda_G$. Accordingly, A can be varied by acting on the temperatures of the two devices. In the achievable range of A ($5\% < A < 8\%$), the VECSEL operates in the regime of passive mode locking. When the pumping level J reaches the threshold value J_{th}, periodic pulses at a period of 2τ are emitted. For increasing J, fundamental mode locking gives way to harmonic mode locking with an increasing number of regularly spaced pulses per round-trip. For $A \approx 5\%$, the pulse instability predicted theoretically is observed in several ranges of values of J. In Fig. 5 we provide experimental evidence of this instability in the situation where two pulses are present in the same round-trip. We plot their evolution as a function of the number of cavity round-trips together with the time-average optical spectrum. The satellite instability affects each pulse in antiphase, leading to their explosion as described in Figs. 4(d), 4(e), 4(f). We believe that the instability described in Ref. [40] has the same origin.

In conclusion, we discussed in this Letter how second and third order dispersion can be implemented in delayed dynamical systems using delay algebraic equations and how this particular dynamical system appears naturally as a boundary condition on a partially reflecting microcavity. The functional mapping method previously developed allowed us to find, in the linear regime, the equivalent partial differential equation for the field evolution which allows linking the eigenvalue spectrum with the coefficient of the third order dispersion. We exemplified the influence of third order dispersion on the dynamics of pulses found in a mode-locked semiconductor laser and we have found that satellites may grow into a fully developed mode-locked pulse that eventually replaces the original pulse. Our experimental results are in good agreement with theory.

We acknowledge fruitful discussions with A. Vladimirov and A. Pimenov. C. S., S. G., and J. J. acknowledge financial support from projects COMBINA (TEC2015-65212-C3-3-P AEI/FEDER UE) and MOVELIGHT (PGC2018-099637-B-100 AEI/FEDER UE). S. G. and J. J. thank the PRIME programme of the German Academic Exchange Service (DAAD) with funds from the German Federal Ministry of Education and Research (BMBF). This work was partially supported by the French RENATECH network, the ANR-18-CE24-0002 BLASON and Conseil Régional Provence-Alpes-Côte d'Azur (plateforme OPTIMAL).

*Corresponding author.
gurevics@uni-muenster.de

[1] G. Giacomelli, F. Marino, M. A. Zaks, and S. Yanchuk, Nucleation in bistable dynamical systems with long delay, Phys. Rev. E **88**, 062920 (2013).
[2] L. Larger, B. Penkovsky, and Y. Maistrenko, Virtual Chimera States for Delayed-Feedback Systems, Phys. Rev. Lett. **111**, 054103 (2013).
[3] F. Marino, G. Giacomelli, and S. Barland, Front Pinning and Localized States Analogues in Long-Delayed Bistable Systems, Phys. Rev. Lett. **112**, 103901 (2014).
[4] M. Marconi, J. Javaloyes, S. Balle, and M. Giudici, How Lasing Localized Structures Evolve Out of Passive Mode Locking, Phys. Rev. Lett. **112**, 223901 (2014).
[5] M. Marconi, J. Javaloyes, S. Barland, S. Balle, and M. Giudici, Vectorial dissipative solitons in vertical-cavity surface-emitting lasers with delays, Nat. Photonics **9**, 450 (2015).
[6] B. Garbin, J. Javaloyes, G. Tissoni, and S. Barland, Topological solitons as addressable phase bits in a driven laser, Nat. Commun. **6**, 5915 (2015).
[7] S. Yanchuk and G. Giacomelli, Dynamical systems with multiple long-delayed feedbacks: Multiscale analysis and spatiotemporal equivalence, Phys. Rev. E **92**, 042903 (2015).
[8] S. Yanchuk and G. Giacomelli, Pattern Formation in Systems with Multiple Delayed Feedbacks, Phys. Rev. Lett. **112**, 174103 (2014).
[9] G. Giacomelli and A. Politi, Relationship between Delayed and Spatially Extended Dynamical Systems, Phys. Rev. Lett. **76**, 2686 (1996).
[10] S. Yanchuk and G. Giacomelli, Spatio-temporal phenomena in complex systems with time delays, J. Phys. A **50**, 103001 (2017).
[11] A. Pimenov, S. Slepneva, G. Huyet, and A. G. Vladimirov, Dispersive Time-Delay Dynamical Systems, Phys. Rev. Lett. **118**, 193901 (2017).
[12] F. Leo, S. Coen, P. Kockaert, S. P. Gorza, P. Emplit, and M. Haelterman, Temporal cavity solitons in one-dimensional kerr media as bits in an all-optical buffer, Nat. Photonics **4**, 471 (2010).

[13] A. Couairon and J. M. Chomaz, Pattern Selection in the Presence of a Cross Flow, Phys. Rev. Lett. **79**, 2666 (1997).
[14] H. Ward, M. N. Ouarzazi, M. Taki, and P. Glorieux, Influence of walkoff on pattern formation in nondegenerate optical parametric oscillators, Phys. Rev. E **63**, 016604 (2000).
[15] A. Mussot, E. Louvergneaux, N. Akhmediev, F. Reynaud, L. Delage, and M. Taki, Optical Fiber Systems are Convectively Unstable, Phys. Rev. Lett. **101**, 113904 (2008).
[16] M. Tlidi, L. Bahloul, L. Cherbi, A. Hariz, and S. Coulibaly, Drift of dark cavity solitons in a photonic-crystal fiber resonator, Phys. Rev. A **88**, 035802 (2013).
[17] F. Leo, A. Mussot, P. Kockaert, P. Emplit, M. Haelterman, and M. Taki, Nonlinear Symmetry Breaking Induced by Third-Order Dispersion in Optical Fiber Cavities, Phys. Rev. Lett. **110**, 104103 (2013).
[18] P. Parra-Rivas, D. Gomila, F. Leo, S. Coen, and L. Gelens, Third-order chromatic dispersion stabilizes Kerr frequency combs, Opt. Lett. **39**, 2971 (2014).
[19] A. G. Vladimirov and D. Turaev, Model for passive mode locking in semiconductor lasers, Phys. Rev. A **72**, 033808 (2005).
[20] H. A. Haus, Mode-locking of lasers, IEEE J. Sel. Top. Quantum Electron. **6**, 1173 (2000).
[21] M. Heuck, S. Blaaberg, and J. Mørk, Theory of passively mode-locked photonic crystal semiconductor lasers, Opt. Express **18**, 18003 (2010).
[22] S. Yanchuk, L. Lücken, M. Wolfrum, and A. Mielke, Spectrum and amplitude equations for scalar delay-differential equations with large delay, Discrete Contin. Dyn. Syst. **35**, 537 (2015).
[23] See Supplemental Material at http://link.aps.org/supplemental/10.1103/PhysRevLett.123.043902 for an analytical approximation of the eigenvalues of Eq. (1) leading to the diffusion and dispersion coefficients of the partial differential equation given by Eq. (10), as well as a detailed discussion of the experimental setup.
[24] The sign of the third order dispersion can be inverted by setting $\mathbf{M}_\varepsilon \to -\mathbf{M}_\varepsilon$.
[25] J. Mulet and S. Balle, Mode locking dynamics in electrically-driven vertical-external-cavity surface-emitting lasers, IEEE J. Quantum Electron. **41**, 1148 (2005).
[26] M. Marconi, J. Javaloyes, S. Balle, and M. Giudici, Passive mode-locking and tilted waves in broad-area vertical-cavity surface-emitting lasers, IEEE J. Sel. Top. Quantum Electron. **21**, 85 (2015).
[27] C. Schelte, J. Javaloyes, and S. V. Gurevich, Functional mapping for passively mode-locked semiconductor lasers, Opt. Lett. **43**, 2535 (2018).
[28] P. Camelin, C. Schelte, A. Verschelde, A. Garnache, G. Beaudoin, I. Sagnes, G. Huyet, J. Javaloyes, S. V. Gurevich, and M. Giudici, Temporal localized structures in mode-locked vertical external-cavity surface-emitting lasers, Opt. Lett. **43**, 5367 (2018).
[29] F. Gires and P. Tournois, Interferometre utilisable pour la compression d'impulsions lumineuses modulees en frequence, C.R. Hebd. Seances Acad. Sci. **258**, 6112 (1964).
[30] S. T. Cundiff, J. M. Soto-Crespo, and N. Akhmediev, Experimental Evidence for Soliton Explosions, Phys. Rev. Lett. **88**, 073903 (2002).
[31] S. C. V. Latas and M. F. S. Ferreira, Soliton explosion control by higher-order effects, Opt. Lett. **35**, 1771 (2010).
[32] A. F. J. Runge, N. G. R. Broderick, and M. Erkintalo, Observation of soliton explosions in a passively mode-locked fiber laser, Optica **2**, 36 (2015).
[33] C. Cartes and O. Descalzi, Periodic exploding dissipative solitons, Phys. Rev. A **93**, 031801(R) (2016).
[34] S. V. Gurevich, C. Schelte, and J. Javaloyes, Impact of high-order effects on soliton explosions in the complex cubic-quintic Ginzburg-Landau equation, Phys. Rev. A **99**, 061803 (2019).
[35] J. Javaloyes, P. Camelin, M. Marconi, and M. Giudici, Dynamics of Localized Structures in Systems with Broken Parity Symmetry, Phys. Rev. Lett. **116**, 133901 (2016).
[36] P. Camelin, J. Javaloyes, M. Marconi, and M. Giudici, Electrical addressing and temporal tweezing of localized pulses in passively-mode-locked semiconductor lasers, Phys. Rev. A **94**, 063854 (2016).
[37] A. Laurain, M. Myara, G. Beaudoin, I. Sagnes, and A. Garnache, Multiwatt-power highly-coherent compact single-frequency tunable vertical-external-cavity-surface-emitting-semiconductor-laser, Opt. Express **18**, 14627 (2010).
[38] B. Chomet, J. Zhao, L. Ferrieres, M. Myara, G. Guiraud, G. Beaudoin, V. Lecocq, I. Sagnes, N. Traynor, G. Santarelli, S. Denet, and A. Garnache, High-power tunable low-noise coherent source at 1.06 μm based on a surface-emitting semiconductor laser, Appl. Opt. **57**, 5224 (2018).
[39] A. Garnache, S. Hoogland, A. C. Tropper, I. Sagnes, G. Saint-Girons, and J. S. Roberts, Sub-500-fs soliton-like pulse in a passively mode-locked broadband surface-emitting laser with 100 mW average power, Appl. Phys. Lett. **80**, 3892 (2002).
[40] T. Malica, J. Lin, T. Ackemann, D. J. Little, J. P. Toomey, D. Pabœuf, W. Lubeigt, N. Hempler, G. Malcolm, G. T. Maker, and D. M. Kane, Mapping the dynamical regimes of a sesam mode-locked vecsel with a long cavity using time series analysis, Opt. Express **26**, 16624 (2018).